OPTIMAL CONTROL APPLICATIONS AND METHODS
Optim. Control Appl. Meth., 2004; **25**:67–89 (DOI: 10.1002/oca.739)

Optimal patterns of glider dynamic soaring

Yiyuan J. Zhao*,†,‡

Department of Aerospace Engineering and Mechanics, University of Minnesota, Minneapolis, MN 55455-0729, U.S.A.

SUMMARY

This paper presents optimal patterns of glider dynamic soaring utilizing wind gradients. A set of three-dimensional point-mass equations of motion is used and basic glider performance parameters are identified through normalizations of these equations. In particular, a single parameter is defined that represents the combined effects of air density, glider wing loading, and wind gradient slope. Glider dynamic soaring flights are formulated as non-linear optimal control problems and three performance indices are considered. In the first formulation, the completion time of one cycle of dynamic soaring is minimized subject to glider equations of motion, limitations on glider flights, and appropriate terminal constraints that enforce a periodic dynamic soaring flight. In the second formulation, the final altitude after one cycle of dynamic soaring is maximized subject to similar constraints. In the third formulation, the least required wind gradient slope that can sustain an energy-neutral dynamic soaring flight is determined. Different terminal constraints are used to produce basic, travelling, and loiter dynamic soaring patterns. These optimal control problems are converted into parameter optimization via a collocation approach and solved numerically with the software NPSOL. Different patterns of glider dynamic soaring are compared in terms of cycle completion time and altitude-increasing capability. Effects of wind gradient slope and wind profile non-linearity on dynamic soaring patterns are examined. Copyright © 2004 John Wiley & Sons, Ltd.

KEY WORDS: dynamic soaring; optimal control; glider; wind gradient

1. INTRODUCTION

Dynamic soaring is the art of powerless flight by utilizing wind gradients over altitudes. Some birds have evolved ways of using the wind gradient to save energy. In doing so, they need to fly very close to the ground or water, where the gradient is often the steepest. In early days of glider soaring, there were many attempts at dynamic soaring in hill updraft with varying degree of success. Due to the closeness to the ground or water surface, a glider pilot trying to imitate the birds would find it arduous and may need to be ever watchful of any change of wind. With advances in glider design and performances over the last several decades, it is time that the potential benefits of dynamic soaring be studied again.

*Correspondence to: Yiyuan J. Zhao, Department of Aerospace Engineering and Mechanics, University of Minnesota, 110 Umon Street St., Minneapolis, MN 55455-0729, U.S.A.
†E-mail: gyyz@aem.umn.edu
‡Associate Professor, Aerospace Engineering and Mechanics

Received 9 April 2003
Revised 19 December 2003
Accepted 11 March 2004

In addition, unmanned aerial vehicles (UAV) are finding a wide range of applications. Unmanned gliders may be controlled automatically to utilize wind gradients to accomplish missions. In these applications, fundamental considerations will be different from those for manned gliding flights. Accordingly, potential dynamic soaring patterns and their performance characteristics may need to examined.

Figure 1 shows two patterns of dynamic soaring [1]. In the first pattern as shown in Figure 1(a), a glider would dive along the wind direction until it is very close to the ground or water to gain speed. It would then make a climbing turn into the wind gradient while losing speed. The glider would then make a further turn and dive down again to repeat the process. If the wind gradient is sufficiently steep, the energy extracted from it by the glider may be adequate to

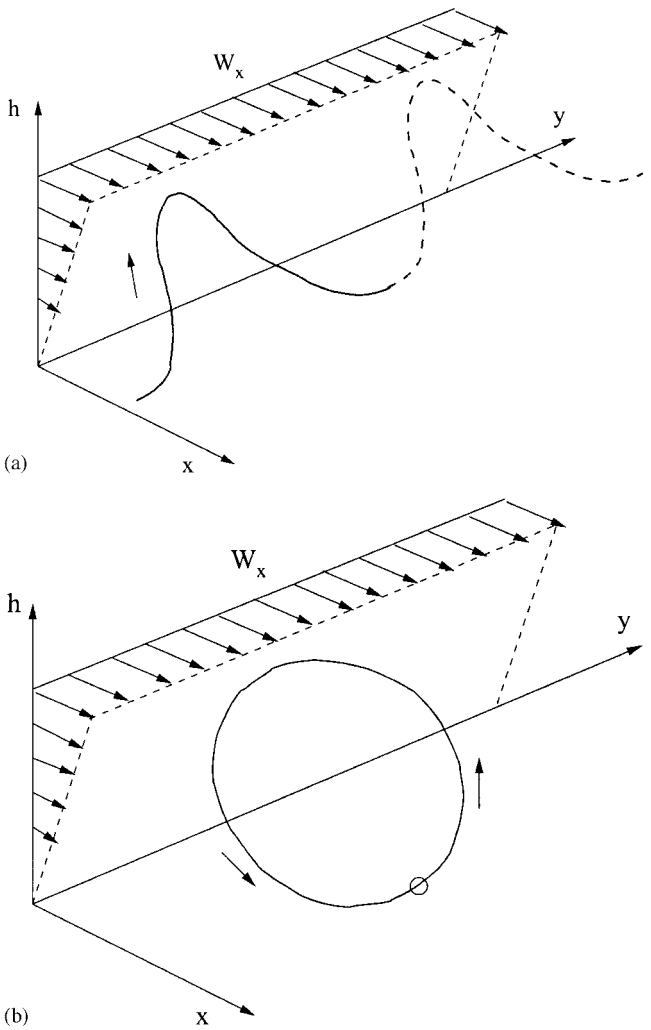

Figure 1. Dynamic soaring: (a) travelling pattern; and (b) loiter pattern.

overcome the drag for continuous flight. In the second pattern as shown in Figure 1(b), a glider would dive across the wind gradient, then climb into the wind, and then turn and dive again, for powerless sustained loiter flight.

In the past, optimization methods have been used to study flight trajectories of glider [2–16]. In particular in Reference [15], Sachs *et al*. formulated glider dynamic soaring as an optimal control problem that maximizes the final altitude after a cycle of dynamic soaring, and obtained numerical solutions for a wide range of glider parameters and wind gradient slopes. In Reference [16], Kawabe and Goto examined effectiveness of different numerical solution methods for optimal control problems using a similar formulation and a different glider model.

This paper extends the work in Reference [15] by considering additional optimal control performance indices and different terminal constraints. These different formulations yield three patterns of dynamic soaring flights: basic, travelling, and loiter. These different patterns of dynamic soaring flights may be used in different UAV missions. In addition, normalized equations are developed and a single parameter is identified that represents the combined effects of air density, wing loading, and average wind gradient. This makes it much easier to quantify relative effects of wind gradients on glider soaring performances. Furthermore, a non-linear wind profile model is presented and effects of different wind gradient profiles are systematically examined.

2. A WIND PROFILE MODEL

With no loss of generality, it is assumed that only the horizontal wind component $W_x(h)$ is present and is a function of altitude. It blows into the East and is stationary. Mean velocity profiles of actual wind gradients can be logarithmic, exponential, or approximately linear [17,18]. A wind gradient model is developed below that can represent a linear wind gradient profile, as well as approximate either the logarithmic or exponential wind profile with a certain average wind gradient slope.

Define the average wind gradient slope as

$$\beta = \frac{W_{x,\max}}{h_{\mathrm{tr}}} \tag{1}$$

where $W_{x,\max}$ is the maximum horizontal wind and h_{tr} is the transition altitude at which the horizontal wind becomes constant with respect to altitude. Further define

$$\tilde{W}_x \triangleq \frac{W_x}{W_{x,\max}}, \quad \tilde{h} \triangleq \frac{h}{h_{\mathrm{tr}}} \tag{2}$$

A linear wind gradient profile can then be expressed as

$$W_x = \beta h \quad \text{or} \quad \tilde{W}_x = \tilde{h} \tag{3}$$

Consider a quadratic variation of the linear profile

$$\tilde{W}_x = A\tilde{h} + (1 - A)\tilde{h}^2 \tag{4}$$

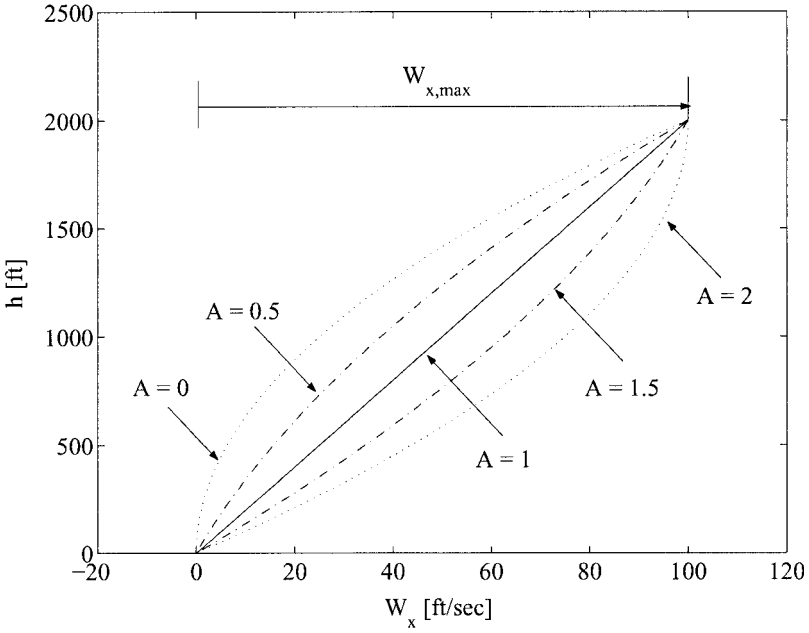

Figure 2. Wind gradient profiles.

where $\tilde{W}_x = 0$ at $\tilde{h} = 0$ and $\tilde{W}_x = 1$ at $\tilde{h} = 1$. Substituting Equation (2) into Equation (4), we have

$$W_x = \frac{W_{x,\max}}{h_{\text{tr}}}\left[Ah + \frac{1-A}{h_{\text{tr}}}h^2\right] = \beta\left[Ah + \frac{1-A}{h_{\text{tr}}}h^2\right] \tag{5}$$

This wind profile has an average slope of β over $[0,h_{\text{tr}}]$. In order to ensure that the wind component is within $[0,W_{x,\max}]$, it is required that $0<A<2$. Specifically, $0<A<1$ corresponds to an exponential-like wind profile and $1<A<2$ corresponds to a logarithmic-like wind profile. At $A=1$, the wind profile becomes a straight line (Figure 2).

3. EQUATIONS OF MOTION AND GLIDER MODELS

A point-mass model is adequate for the study of optimal glider flight trajectories. With the assumption of a flat earth and stationary winds, a three-dimensional point-mass equations of motion for a generic glider can be derived as follows:

$$m\dot{V} = -D - mg\sin\gamma - m\dot{W}_x\cos\gamma\sin\Psi \tag{6}$$

$$mV\cos\gamma\,\dot{\Psi} = L\sin\mu - m\dot{W}_x\cos\Psi \tag{7}$$

$$mV\dot{\gamma} = L\cos\mu - mg\cos\gamma + m\dot{W}_x \sin\gamma \sin\Psi \tag{8}$$

$$\dot{h} = V\sin\gamma \tag{9}$$

$$\dot{x} = V\cos\gamma\sin\Psi + W_x(h) \tag{10}$$

$$\dot{y} = V\cos\gamma\cos\Psi \tag{11}$$

In the above, m is the glider mass, V is the airspeed, Ψ is the heading angle measured clockwise from the North, γ is the air-relative flight path angle, h is the altitude, (x,y) are (East, North) position, W_x is the wind component along the East direction, μ is the glider bank angle, L is the lift force, and D is the drag force. We have

$$L = \tfrac{1}{2}\rho V^2 S C_L, \quad D = \tfrac{1}{2}\rho V^2 S C_D, \quad C_D = C_{D_0} + KC_L^2 \tag{12}$$

where (C_L,C_D) are the (lift,drag) coefficient, C_{D_0} is the parasitic drag coefficient, and K is the induced drag factor, which can be conveniently expressed as a function of the parasitic drag coefficient and the best lift-to-drag ratio $E_{\max}$ as

$$K = \frac{1}{4E_{\max}^2 C_{D_0}} \tag{13}$$

where

$$E_{\max} = \left(\frac{C_L}{C_D}\right)_{\max} = \left(\frac{C_L}{C_{D_0} + KC_L^2}\right)_{\max} \tag{14}$$

The time rate of change of the stationary horizontal wind component W_x is caused by glider motion and can be determined from

$$\dot{W}_x = \frac{\partial W_x}{\partial h}\dot{h} = \beta\left[A + 2\frac{1-A}{h_{\text{tr}}}h\right] V\sin\gamma \tag{15}$$

In this set of equations, the glider mass is assumed to be constant and the lift coefficient is used as a control variable. For an actual glider, the lift coefficient is primarily a function of the angle of attack, and can be effected through the elevator motion, which has a much faster response than the trajectory motion.

To enhance the efficiency of numerical solutions, the above equations are normalized as follows. Define

$$\bar{V} = \frac{V}{g/\beta}, \quad (\bar{x},\bar{y},\bar{h}) = \frac{x,y,h}{g/\beta^2}, \quad \tau = \beta t \tag{16}$$

and

$$\frac{\mathrm{d}(\,)}{\mathrm{d}\tau} = (\,)' = \frac{1}{\beta}\frac{\mathrm{d}(\,)}{\mathrm{d}t} = \frac{1}{\beta}(\dot{\,}) \tag{17}$$

After some derivations, the normalized equations of motion are obtained as

$$\bar{V}' = \bar{T} - \bar{\rho}\bar{V}^2(C_{D_0} + KC_L^2) - \sin\gamma - (A + 2B\bar{h})\bar{V}\sin\gamma\cos\gamma\sin\Psi \tag{18}$$

$$\Psi' = \bar{\rho}\bar{V}\frac{C_L\sin\mu}{\cos\gamma} - (A + 2B\bar{h})\tan\gamma\cos\Psi \tag{19}$$

$$\gamma' = \bar{\rho}\bar{V}C_L\cos\mu - \frac{\cos\gamma}{\bar{V}} + (A + 2B\bar{h})\sin^2\gamma\sin\Psi \tag{20}$$

$$\bar{h}' = \bar{V}\sin\gamma \tag{21}$$

$$\bar{x}' = \bar{V}\cos\gamma\sin\Psi + (A\bar{h} + B\bar{h}^2) \tag{22}$$

$$\bar{y}' = \bar{V}\cos\gamma\cos\Psi \tag{23}$$

where

$$B = \frac{1 - A}{\bar{h}_{\mathrm{tr}}} \qquad \bar{h}_{\mathrm{tr}} = \frac{h_{\mathrm{tr}}}{g/\beta^2} = \frac{\beta^2 h_{\mathrm{tr}}}{g} \tag{24}$$

and

$$\bar{\rho} = \frac{\rho g^2}{2(mg/S)\beta^2} \tag{25}$$

The total specific air-relative energy can be defined as

$$e_{\mathrm{T}} = h + \frac{V^2}{2g} = e_{\mathrm{p}} + e_{\mathrm{k}}$$

where e_{p} is the potential energy component and e_{k} is the kinetic energy component. Their normalized counterparts are given by

$$\bar{e}_{\mathrm{T}} = \bar{h} + \frac{\bar{V}^2}{2} = \bar{e}_{\mathrm{p}} + \bar{e}_{\mathrm{k}} \tag{26}$$

In addition, the normalized energy rate is given by

$$\begin{aligned}\bar{e}'_{\mathrm{T}} &= \bar{h}' + \bar{V}\bar{V}' = \bar{e}'_{\mathrm{drag}} + \bar{e}'_{\mathrm{wind}} \\ &= -\bar{\rho}\bar{V}^3(C_{D_0} + KC_L^2) - (A + 2B\bar{h})\bar{V}^2\sin\gamma\cos\gamma\sin\Psi\end{aligned} \tag{27}$$

where $\bar{e}'_{\mathrm{drag}}$ is caused by the aerodynamic drag, and $\bar{e}'_{\mathrm{wind}}$ is caused by the wind.

Symbolically, the normalized equations of motion can be expressed as

$$\mathbf{x}' = f(\mathbf{x}, \mathbf{u}) \tag{28}$$

where $\mathbf{x}$ is the state vector and $\mathbf{u}$ is the control vector.

$$\mathbf{x} = \begin{bmatrix} \bar{V} \\ \Psi \\ \gamma \\ \bar{h} \\ \bar{x} \\ \bar{y} \end{bmatrix}, \quad \mathbf{u} = \begin{bmatrix} C_L \\ \mu \end{bmatrix} \tag{29}$$

The above normalized equations reveal three essential performance parameters for glider flights through a wind gradient: $\bar{\rho}$, C_{D_0}, and $E_{\max}$, where $\bar{\rho}$ incorporates the combined effects of atmospheric density, wing loading, and wind gradient slope, and is the fundamental parameter describing the relative intensity of a wind gradient profile for a given glider. In comparison, (C_{D_0},$E_{\max}$) represent the aerodynamic properties of a glider. It is assumed

$$C_{D,0} = 0.005 - 0.015, \qquad E_{\max} = 20 - 80 \tag{30}$$

4. OPTIMAL CONTROL PROBLEM FORMULATIONS

Three optimal control problems are now formulated. Each problem formulation can be equipped with different terminal constraints to obtain different patterns of dynamic soaring.

4.1. Dynamic soaring with minimum cycle time

The first problem seeks to minimize the completion time of one dynamic soaring cycle. The minimum cycle time problem is meaningful to determine ranges of feasible UAV flight times. Mathematically,

$$\min_{C_L,\mu;\bar{V}_0,\Psi_0,\tau_f} I = \tau_f \tag{31}$$

subject to Equations (18)–(23), the following initial conditions:

$$\bar{x}(0) = 0 \tag{32}$$

$$\bar{y}(0) = 0 \tag{33}$$

$$\bar{h}(0) = 0 \tag{34}$$

$$\gamma(0) = 0 \tag{35}$$

the following path constraints:

$$\bar{h} \geqslant 0 \tag{36}$$

$$C_{L_{\min}} \leqslant C_L \leqslant C_{L_{\max}} \tag{37}$$

$$-\mu_{\max} \leqslant \mu \leqslant \mu_{\max} \tag{38}$$

$$n = \frac{L}{mg} \leqslant n_{\max} \tag{39}$$

and appropriate terminal constraints. In this problem, the initial airspeed and heading angle are open. This will permit the optimization process to determine their optimal values for sustainable soaring flights. The initial flight path angle is set to be zero in Equation (35), because a periodic flight will always have a point where the flight path angle is zero.

The first set of terminal constraints are selected to enforce a *basic dynamic soaring* flight,

$$\bar{V}(\tau_f) = \bar{V}(0) \tag{40}$$

$$\Psi(\tau_f) = \Psi(0) \tag{41}$$

$$\gamma(\tau_f) = \gamma(0) \tag{42}$$

$$\bar{h}(\tau_f) = \bar{h}(0) + \Delta\bar{H} \tag{43}$$

where $\Delta\bar{H}$ is a specified amount of altitude increase at the end of each dynamic soaring cycle. In particular, $\Delta\bar{H} = 0$ leads to energy-neutral dynamic soaring. In order to achieve a *travelling dynamic soaring*, the following terminal constraint is added:

$$\bar{x}(\tau_f) = \bar{x}(0) \tag{44}$$

Finally, a *loiter dynamic soaring* flight can be studied by including all of the above terminal constraints as well as the following one:

$$\bar{y}(\tau_f) = \bar{y}(0) \tag{45}$$

4.2. Dynamic soaring with maximum altitude gain per cycle

In the second problem formulation, the altitude-increasing capability of flying through a wind gradient region is studied through

$$\max_{C_L,\mu;\bar{V}_0,\Psi_0,\tau_f} I = \bar{h}(\tau_f) \tag{46}$$

subject to Equations (18)–(23), initial conditions in Equations (32)–(35), the path constraints in Equations (36)–(39), and appropriate terminal constraints discussed above where the final

altitude constraint in Equation (43) is removed. This performance index with terminal constraints in Equations (40)–(42) is the same problem formulation used in Reference [15], and is similar to the problem formulation in Reference [16].

Actually, the maximum final altitude problem and the minimum cycle time problem produce consistent optimal dynamic soaring trajectories, as shown below.

4.3. Least required wind gradient slope for soaring flights

Finally, an optimal control problem is formulated to determine the least required slope of a linear wind gradient profile that can still sustain a powerless dynamic soaring flight,

$$\max_{C_L,\mu;\bar{V}_0,\Psi_0,\tau_f,\bar{\rho}} I = \bar{\rho} \tag{47}$$

subject to Equations (18)–(23), initial conditions in Equations (32)–(35), the path constraints in Equations (36)–(39), and appropriate terminal constraints as discussed in the minimum cycle time formulation.

5. NUMERICAL SOLUTIONS OF DYNAMIC SOARING PROBLEMS

The above formulations constitute periodic optimal control problems [19]. In this paper, these problems are solved numerically with a collocation approach [20–22], in which both state and control variables are parameterized. The resulting parameter optimization problems are solved with the software package NPSOL [23]. Details are now explained.

5.1. Parameterization of non-linear optimal control problems

The conversion of an optimal control problem into parameter optimization using the collocation approach begins with the definition of a series of N time points within the solution time interval $[0,\tau_f]$. Define

$$0 = \bar{\tau}_1 < \bar{\tau}_2 < \cdots < \bar{\tau}_{N-1} < \bar{\tau}_N = 1 \tag{48}$$

Then

$$\tau_k = \tau_f \bar{\tau}_k, \quad k = 1, 2, \ldots, N \tag{49}$$

In case of equally spaced points

$$\bar{\tau}_k = \frac{k-1}{N-1}, \quad k = 1, 2, \ldots, N \tag{50}$$

Values of the state and control variables at each time point become solution parameters:

$$x_1^i, \ldots, x_k^i, \ldots, x_N^i \tag{51}$$

$$u_1^j, \ldots, u_k^j, \ldots, u_N^j \tag{52}$$

where $x_k^i = x^i(\tau_k)$ is the ith component of the state vector $\mathbf{x}$ evaluated at τ_k, $i=1,\ldots,6$, and $u_k^j = u^j(\tau_k)$ is the jth component of the control vector $\mathbf{u}$ evaluated at τ_k, $j=1,2$. Putting all of the unknown parameters together, we have,

$$\mathbf{X} = [x_1^1, \ldots, x_N^1, \ldots, x_1^6, \ldots, x_N^6, u_1^1, \ldots, u_N^1, u_1^2, \ldots, u_N^2, \tau_f] \tag{53}$$

which has $8N+1$ variables. For the third optimal control problem in Equation (47), $\bar{\rho}$ needs to be included as an additional solution parameter.

The six differential equations in Equations (18)–(23) are converted into $6(N-1)$ non-linear equality constraints on these solution parameters. For $k=1,2,\ldots,N-1$, define

$$\mathbf{x}_m = \tfrac{1}{2}(\mathbf{x}_k + \mathbf{x}_{k+1}) - \tfrac{1}{8}(f_{k+1} - f_k)(\tau_{k+1} - \tau_k) \tag{54}$$

$$\mathbf{u}_m = \tfrac{1}{2}(\mathbf{u}_k + \mathbf{u}_{k+1}) \tag{55}$$

$$f_{m,k} = f(\mathbf{x}_m, \mathbf{u}_m) \tag{56}$$

where $f_{k+1} = f(\mathbf{x}_{k+1}, \mathbf{u}_{k+1})$ and $f_k = f(\mathbf{x}_k, \mathbf{u}_k)$. Using the Simpson's $\frac{1}{3}$ rule, the resulting equality constraints can be expressed as

$$C_{k+(i-1)(N-1)} = x_{k+1}^i - x_k^i - \tfrac{1}{6}(f_k^i + 4f_{m,k}^i + f_{k+1}^i)(\tau_{k+1} - \tau_k) \tag{57}$$

where f^i is the ith component of the vector function f, $i=1,2,\ldots,6$.

The path constraints in Equations (36)–(39) are enforced at the series of discrete time points as bounds on the solution parameters. Initial state conditions in Equations (32)–(35) are enforced by equating upper and lower bounds on the corresponding variables. Finally, the terminal conditions in Equations (40)–(45) are enforced as linear constraints on solution variables.

The converted parameter optimization problem may then be stated in the following general form:

$$\min_{\mathbf{X}} \; F(\mathbf{X}) \tag{58}$$

subject to

$$\mathbf{L} \leqslant \begin{Bmatrix} \mathbf{X} \\ A_L\mathbf{X} \\ C(\mathbf{X}) \end{Bmatrix} \leqslant \mathbf{U} \tag{59}$$

where $F(\mathbf{X})$ is a non-linear objective function, A_L is a constant matrix of general linear constraints, and $C(\mathbf{X})$ is a vector of non-linear constraint functions. The upper and lower bounds $\mathbf{L}$ and $\mathbf{U}$ are specified for all the solution variables and for all the constraints.

5.2. Overview of the NPSOL program

NPSOL [23] is a suite of Fortran 77 subroutines designed to solve the above non-linear programming problem. The objective function and the constraint functions are assumed to be smooth. Internally, NPSOL uses a sequential quadratic programming algorithm (SQP), in which the search direction is the solution of a quadratic programming subproblem. The step size at each iteration is iteratively selected to produce a sufficient decrease in an augmented Lagrangian merit function. Various features are included to improve the overall efficiency of the SQP algorithm. After a successful convergence, solutions of the NPSOL program represent a local optimal solution to the non-linear programming problem.

5.3. Numerical solution process

In this paper, analytical gradient expressions for both the objective functions and the non-linear constraints are derived. Equally spaced nodes are used. The feasibility and optimality tolerance levels are selected as $\varepsilon_f = 10^{-8}$ and $\varepsilon_o = 10^{-8}$.

Different numbers of the time interval division N are experimented. It is found that a larger N would help the convergence at the expense of longer computational time per iteration. Results presented below are obtained with $N = 31$ for a balance among solution accuracy, convergence, and computational speed. A solution in most cases takes about 50 to 100 iterations.

Proper initial guesses are required to ensure convergence. After extensive numerical experiments, the following initial trajectories are used as the initial guesses.

$$\bar{V}(\tau) = \bar{V}_0\left[1 - 0.5 \sin\frac{\pi\tau}{\tau_f}\right]$$

$$\gamma(\tau) = 80^\circ \sin\frac{2\pi\tau}{\tau_f} \tag{60}$$

$\Psi(\tau) = 0$ for the basic and travelling patterns, and $\Psi(\tau) = -2\pi\tau/\tau_f$ for the loiter pattern. Initial guesses for other state and control variables are constant: $\bar{x}(\tau) = 0$, $\bar{y}(\tau) = 0$, $\bar{h}(\tau) = 0$, $C_L(\tau) = C_{L_0}$, and $\mu(\tau) = 0$. With proper choices of initial guesses of C_{L_0}, τ_f, and $\bar{V}_0$, all problems with linear wind gradient profiles can be made to converge. As long as a problem converges, the solutions are unique. Problems with non-linear wind profiles are solved using converged solutions under linear wind profiles as initial guesses.

5.4. Effectiveness of path constraints

Different bounds on the path constraints in Equations (37)–(39) are studied through numerical solutions. The lift coefficient never becomes negative but does reach the upper bound in a number of solutions. The bank angle constraint in Equation (38) is active during the low speed (or high altitude) portion of a dynamic soaring flight. A smaller value of μ_{max} results in a smaller minimum airspeed and vice versa. In comparison, the constraint on the load factor in Equation (39) affects the maximum airspeed when it is active. On the other hand, the load factor constraint is not active for n_{max} exceeding a certain value (e.g. $n_{max} \geqslant 6$ for the minimum cycle time problem). For different values of μ_{max} and n_{max}, though, salient features of optimal

dynamic soaring trajectories look the same. In the current paper, the following values of flight constraints are used:

$$C_{L_{\min}} = -0.2, \quad C_{L_{\max}} = 1.5, \quad \mu_{\max} = 60^{\circ}, \quad n_{\max} = 5 \tag{61}$$

6. CHARACTERISTICS OF OPTIMAL DYNAMIC SOARING FLIGHTS

We first examine basic characteristics of optimal dynamic soaring flights. In these examples, the following parameters are assumed:

$$C_{D_0} = 0.01, \quad E_{\max} = 40, \quad A = 1.0 \quad \text{and} \quad \bar{\rho} = 100, 80, 60, 40 \tag{62}$$

6.1. Patterns of dynamic soaring with minimum cycle time

Figure 3 shows three patterns of dynamic soaring with minimum cycle time, with $\Delta H = 0$ and $\bar{\rho} = 60$, which corresponds to $\beta = 0.04528\,\mathrm{s}^{-1}$ for $mg/S = 10\,\mathrm{lb/ft}^2$. The corresponding state and control variables are shown in Figure 4. Figure 5 shows energy components and energy rates during a travelling dynamic soaring flight. Energy variations for other patterns of dynamic soaring are similar.

In a typical dynamic soaring flight, the glider would climb into the wind while slowing down to trade kinetic energy for potential energy. It would then descend along the wind while speeding up to trade potential energy for kinetic energy. The total energy stays roughly constant

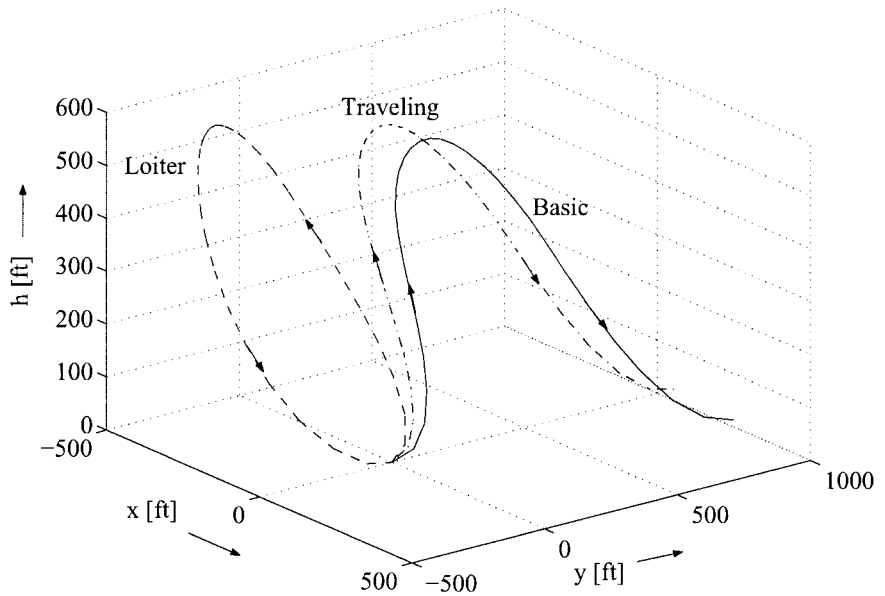

Figure 3. Optimal patterns of minimum cycle time dynamic soaring, $\bar{\rho} = 60$, $C_{D_0} = 0.01$, $E_{\max} = 40$, and $\Delta H = 0$.

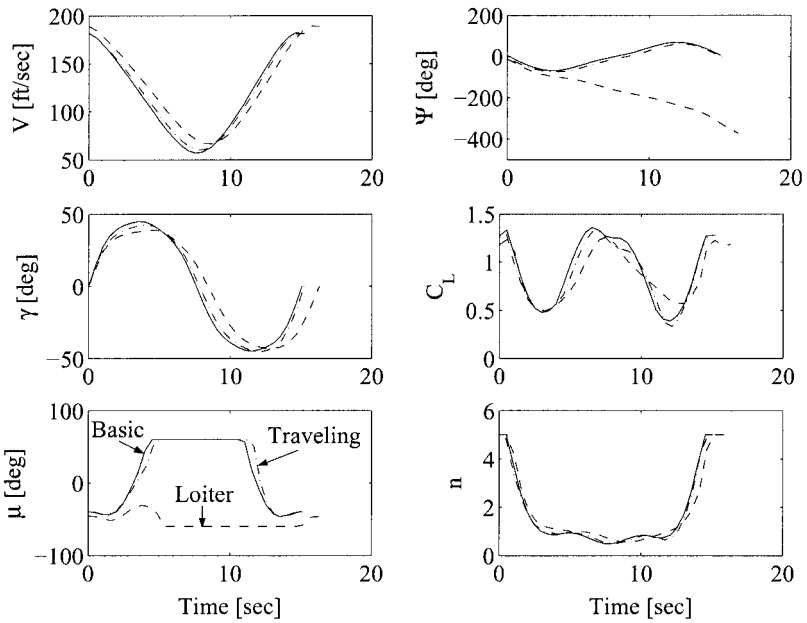

Figure 4. States and controls of minimum cycle time dynamic soaring, $\bar{\rho} = 60$, $C_{D_0} = 0.01$, $E_{\max} = 40$, and $\Delta H = 0$.

during a cycle. Most state and control variables for the three dynamic soaring patterns are similar, with the exceptions of the heading angle and the bank angle. In the basic dynamic soaring pattern, the final glider position is open and the optimal cycle time is determined to be $t_f^* = 15.06$ s. In the travelling dynamic soaring pattern, the final glider position is partially fixed as in Equation (44). The optimal cycle time is determined to be $t_f^* = 15.22$ s. Finally, the loiter dynamic soaring pattern is achieved by completely constraining the final glider position in a cycle, as in Equations (44) and (45). The optimal cycle time is determined to be $t_f^* = 16.28$ s. As shown in Figure 4, the load factor constraint is active at the very beginning and very end of a dynamic soaring cycle, or when the airspeed is highest.

Over a dynamic soaring cycle, the energy dissipated by the drag is compensated by that brought in by flying through the wind profile. The energy rate due to drag is always negative as expected, and is more negative at the lower altitude part of a dynamic soaring cycle when the airspeed is higher. In comparison, the energy rate due to the wind gradient is always positive. It is more positive in the middle of the climb and the descent, and is less positive at the low and high altitude points. Therefore, it can be concluded that consistent wind gradients over the intermediate altitude range is crucial to a successful dynamic soaring flight. This is confirmed below through the examination of the effects of non-linear wind gradient profiles.

6.2. *Effects of wind gradient slope on minimum cycle time soaring*

Figure 6 shows three-dimensional trajectories of the travelling dynamic soaring with minimum cycle time at different $\bar{\rho}'$s, and Figure 7 shows the corresponding state and control variables. Dynamic soaring flights at different wind gradient slopes demonstrate similar characteristics. As

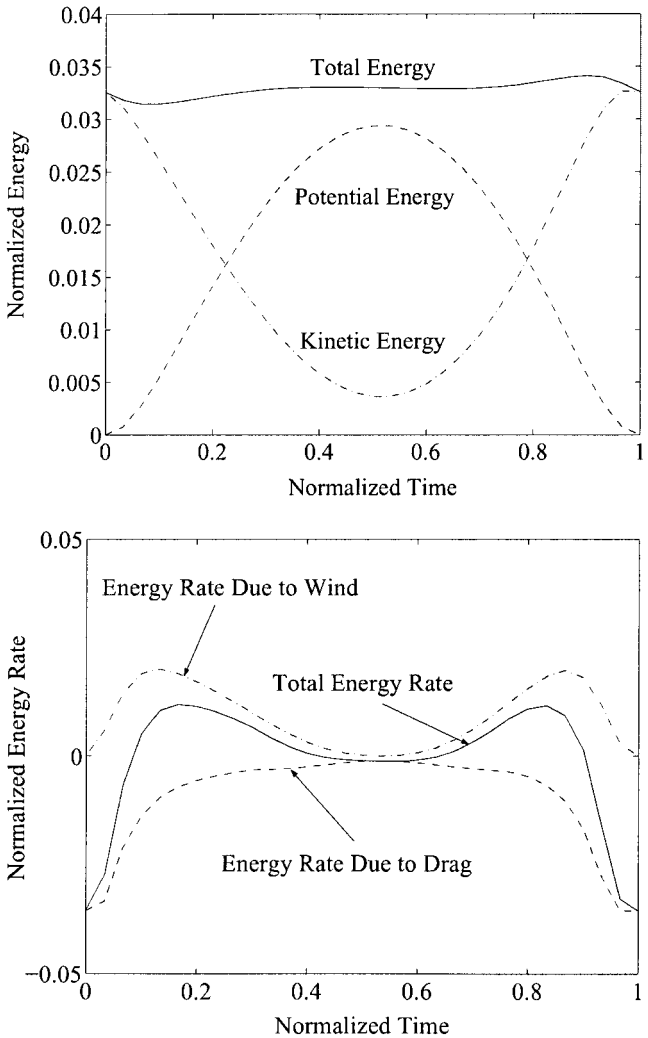

Figure 5. Energy relations in a travelling dynamic soaring with minimum cycle time, $\bar{\rho} = 60$, $C_{D_0} = 0.01$, $E_{\max} = 40$, and $\Delta H = 0$.

$\bar{\rho}$ increases or the wind gradient slope decreases, the optimal cycle time, the peak altitude, and the peak airspeed all increase. In general, the achievable optimal cycle time is a function of the wind gradient slope, the parasitic drag coefficient, and the maximum lift-to-drag ratio. Mathematically, $t_f^* = t_f^*(\bar{\rho}, C_{D_0}, E_{\max})$. Figure 8 shows optimal cycle times at different wind gradient slopes for $C_{D_0} = 0.01$ and $E_{\max} = 40$.

6.3. *Patterns of dynamic soaring with maximum final altitude*

Figure 9 shows three patterns of dynamic soaring with maximum final altitude with $\bar{\rho} = 60$, and Figure 10 shows the corresponding state and control variables. Shapes of dynamic soaring

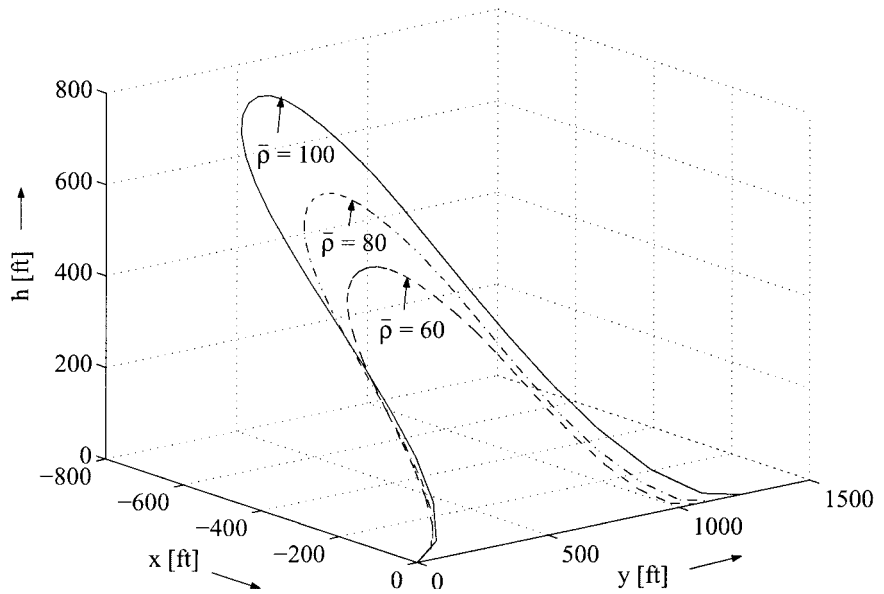

Figure 6. Effects of wind gradient slopes on travelling dynamic soaring with minimum cycle time, $C_{D_0} = 0.01$, $E_{\max} = 40$, and $\Delta H = 0$.

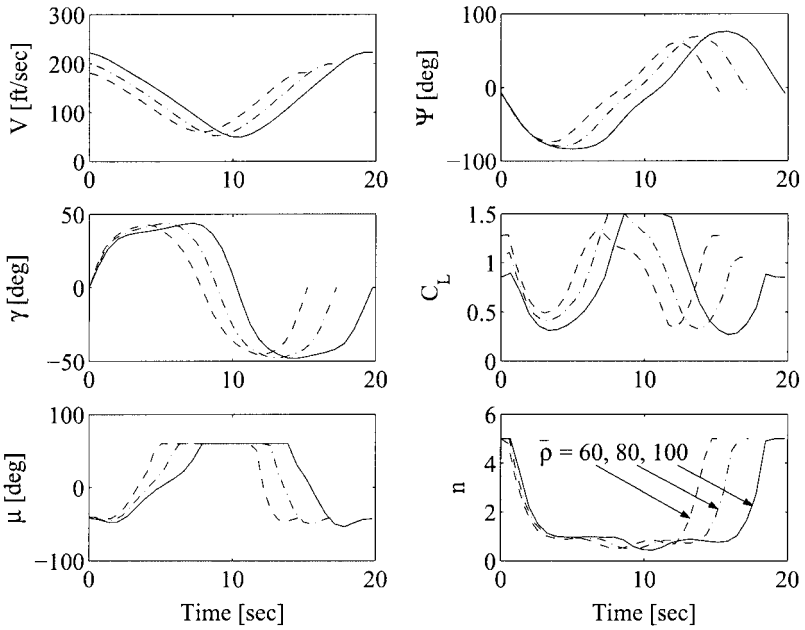

Figure 7. States and controls of travelling dynamic soaring with minimum cycle time, $C_{D_0} = 0.01$, $E_{\max} = 40$, and $\Delta H = 0$.

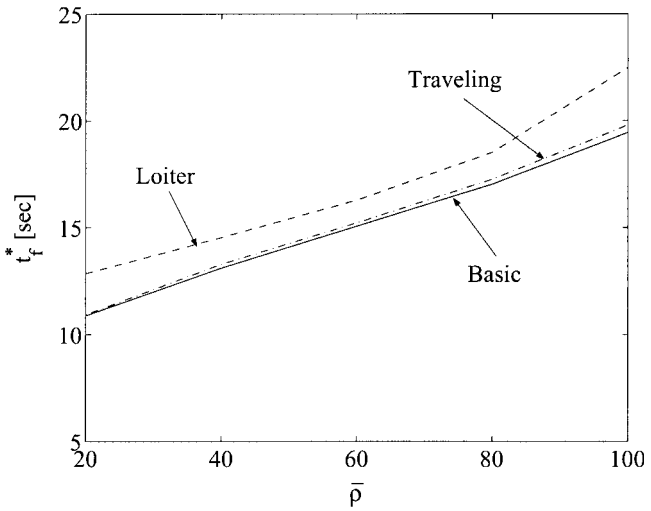

Figure 8. Optimal cycle times of dynamic soaring in different linear wind gradient slopes, $C_{D_0} = 0.01$, $E_{\max} = 40$.

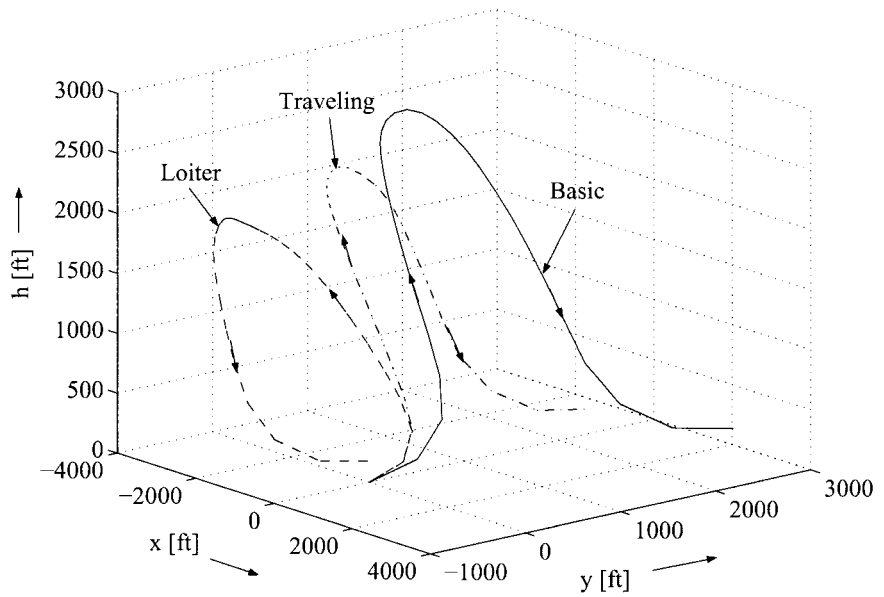

Figure 9. Optimal patterns of maximum final altitude dynamic soaring, $\bar{\rho} = 60$, $C_{D_0} = 0.01$, $E_{\max} = 40$.

trajectories for maximizing the final altitude are similar to those for minimizing the cycle time. On the other hand, cycle times, peak altitudes, and peak airspeeds for the maximum final altitude soaring flights are in general larger than those for the minimum cycle time soaring.

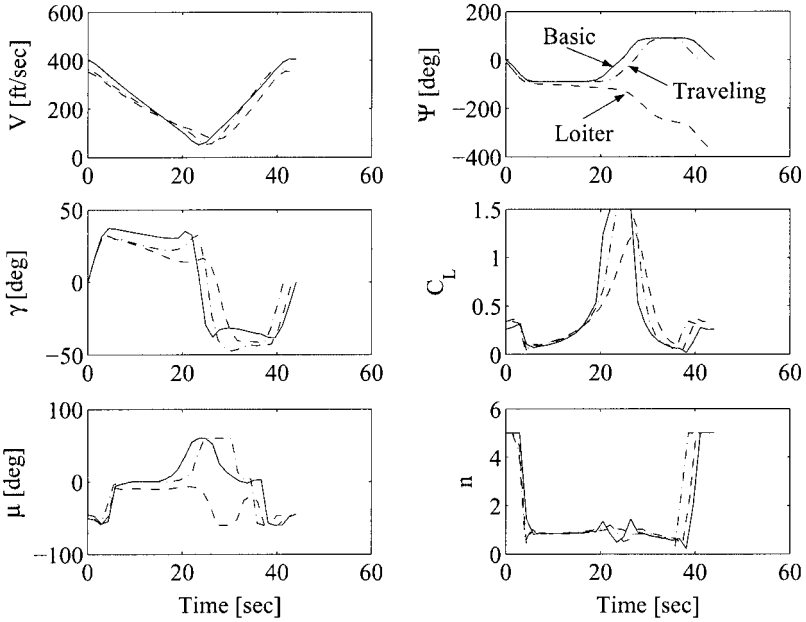

Figure 10. States and controls of maximum final altitude dynamic soaring, $\bar{\rho} = 60$, $C_{D_0} = 0.01$, and $E_{\max} = 40$.

Table I. Final altitude gains per cycle of dynamic soaring, $\bar{\rho} = 60$, $C_{D_0} = 0.01$, $E_{\max} = 40$.

	No constraint on load factor		$n_{\max} = 5$	
	max $h(t_f)$ (ft)	t_f (s)	max $h(t_f)$ (ft)	t_f (s)
Basic	246.46	45.75	110.47	36.39
Travelling	168.63	41.61	92.46	35.25
Loiter	163.92	41.95	69.56	37.56

The basic pattern dynamic soaring trajectories obtained in this paper are consistent with those in References [15,16], When the final x-position is constrained for a travelling dynamic soaring, the possible final altitude gain per cycle becomes less, as shown in Table I. The final altitude gain for the loiter dynamic soaring is even less when both the final x- and the final y-positions are constrained.

Table I summarizes possible altitude gains per cycle in different dynamic soaring patterns, with and without the load factor constraint. Clearly, the inclusion of the load factor constraint significantly affects possible altitude gains in a dynamic soaring pattern. In comparison, the load factor constraint does not affect the minimum cycle times in dynamic soaring as much. The achievable final altitude is in general a function of the wind gradient slope, the parasitic drag

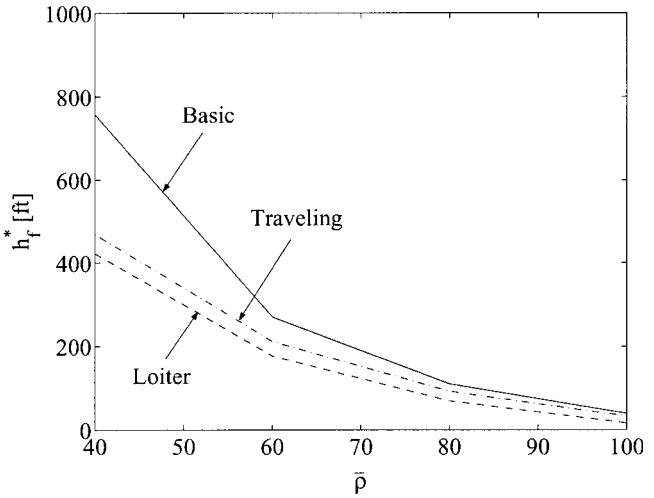

Figure 11. Maximum final altitudes of dynamic soaring in different linear wind gradient slopes, $C_{D_0} = 0.01$, $E_{\max} = 40$.

coefficient, and the aerodynamic efficiency: $h_f^* = h_f^*(\bar{\rho}, C_{D_0}, E_{\max})$. Figure 11 shows achievable final altitude gains per cycle of dynamic soaring at different wind gradient slopes.

6.4. *Relations between the two problem formulations*

The minimum cycle time problem is actually consistent with the maximum final altitude problem. Figure 12 shows trajectories of dynamic soaring with minimum cycle time at four different specified final altitudes. As the specified final altitude is increased, the peak altitude and peak airspeed both increase and the minimum cycle time trajectories gradually approach those of the maximum final altitude dynamic soaring under the same conditions.

7. EFFECTS OF NON-LINEAR WIND PROFILES

In reality, a wind gradient profile is non-linear. Effects of non-linear wind gradient profiles on optimal dynamic soaring flights are now examined. A travelling dynamic soaring pattern is used.

Figure 13 shows the altitude and airspeed histories of the minimum cycle time soaring for a range of non-linear wind profile parameters, with $C_{D_0} = 0.01$ and $E_{\max} = 40$, and for a fixed average wind gradient slope described by $\bar{\rho} = 60$. In comparison, Figure 14 shows similar histories of the maximum final altitude soaring under the same parameter conditions. These results suggest that a larger A produces a smaller optimal cycle time and a higher final altitude. Compared with Figures 8 and 11, a larger A plays a similar role as a larger wind gradient slope (or a smaller $\bar{\rho}$) in the linear wind profile case.

For $A \geqslant 1$, a larger value of A corresponds to a more logarithmic-like wind gradient profile (Figure 2). A logarithmic wind profile has a larger effective wind gradient slope at lower altitudes and a smaller effective wind gradient slope at higher altitudes. The above results

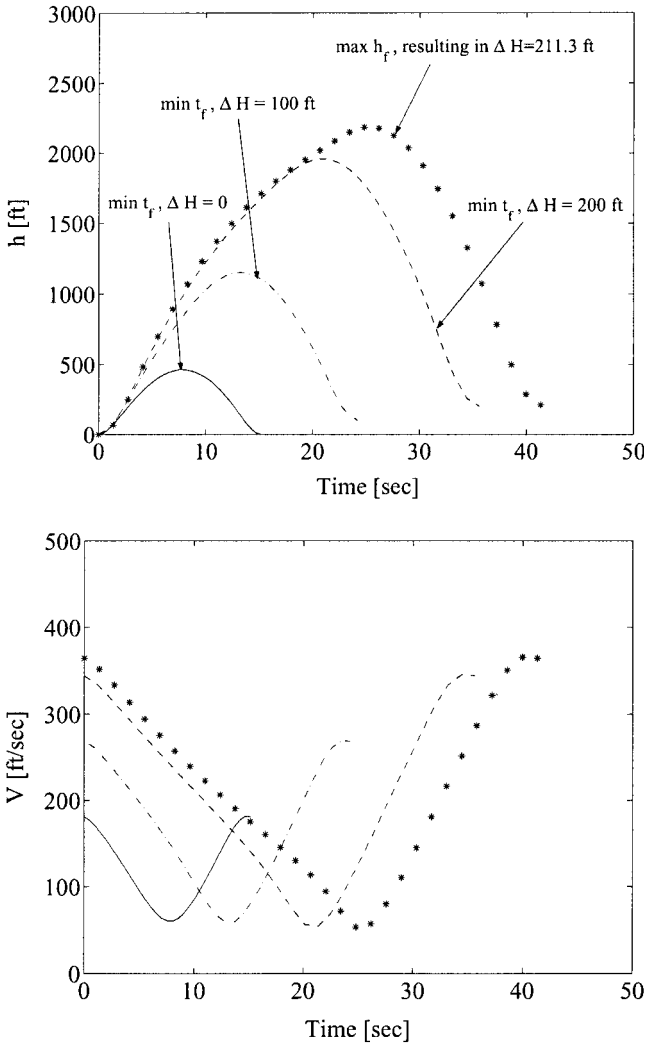

Figure 12. Effects of specified final altitude in travelling dynamic soaring with minimum cycle time, $\bar{\rho} = 60$, $C_{D_0} = 0.01$, $E_{\max} = 40$.

suggest that a larger effective wind gradient slope over the low altitude region is more favourable to a dynamic soaring because this is the region when the vehicle is building up energy reserve (Figure 5). Therefore for a given average wind gradient slope, it is easier for a glider to soar in a more logarithmic-like wind profile. In comparison, $A < 1$ represents an exponential-like wind profile. A smaller value of A corresponds to a smaller effective wind gradient slope over lower altitudes and is thus unfavourable to the dynamic soaring flight. The corresponding optimal cycle time is longer, and the achievable final altitude gain per cycle is smaller.

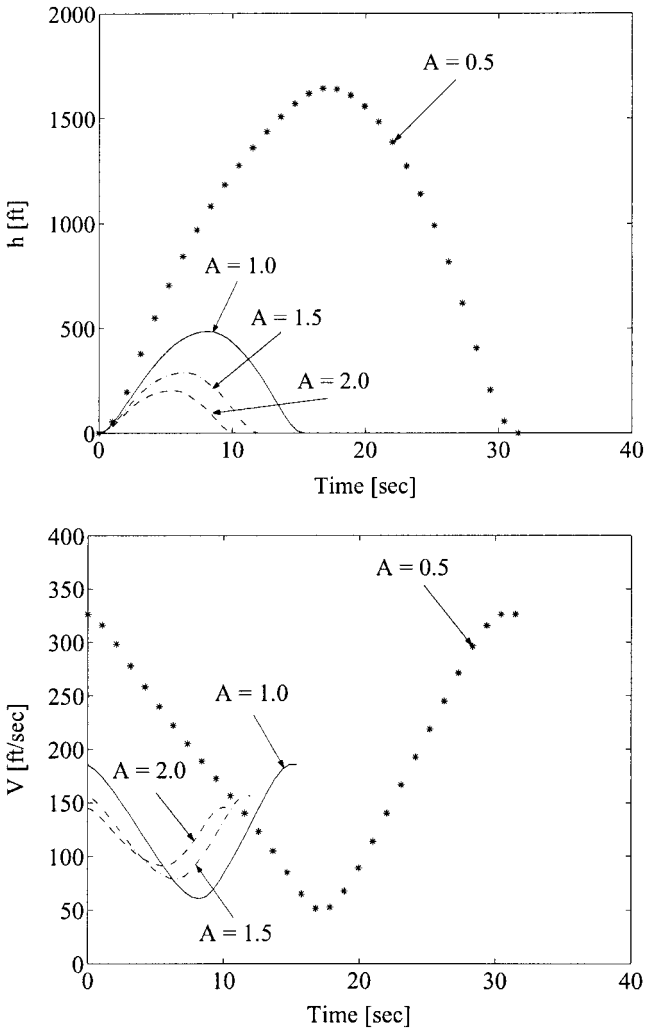

Figure 13. Effects of wind profile non-linearity on travelling dynamic soaring with minimum cycle time, $\bar{\rho} = 60$, $C_{D_0} = 0.01$, $E_{\max} = 40$.

8. LEAST REQUIRED WIND GRADIENT SLOPES FOR SOARING FLIGHTS

When the wind gradient slope becomes smaller than a certain value, sustainable dynamic soaring is no longer possible for a given glider. This least required wind gradient slope corresponds to the maximum feasible value of the normalized parameter $\bar{\rho}$ and depends on the performance parameters of a glider. This value can be determined by the third optimal control problem in Equation (47). In general, $\bar{\rho}_{\max} = \bar{\rho}_{\max}(C_{D_0}, E_{\max})$. Figure 15 shows an example of this result for the basic dynamic soaring problem. As the aerodynamic efficiency $E_{\max}$ is made

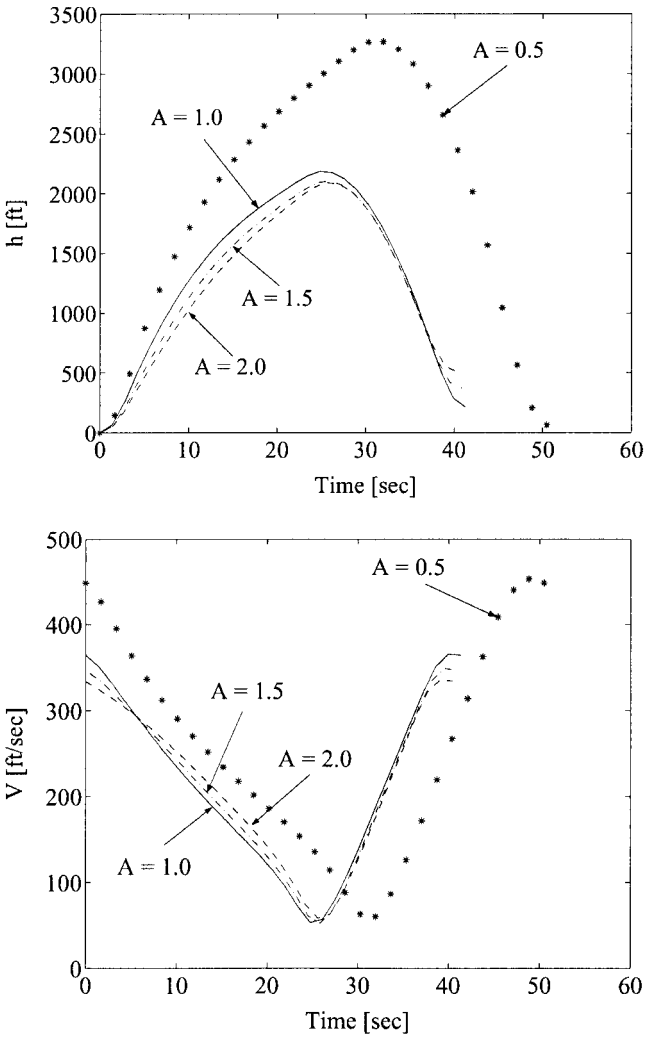

Figure 14. Effects of wind profile non-linearity on travelling dynamic soaring with maximum final altitude, $\bar{\rho} = 60$, $C_{D_0} = 0.01$, $E_{\max} = 40$.

larger or the parasitic drag coefficient C_{D_0} made smaller, it becomes easier for a glider to soar. Correspondingly, the least required wind gradient slope is smaller or $\bar{\rho}_{\max}$ becomes larger.

9. CONCLUSIONS

This paper studies different optimal dynamic soaring patterns of a glider in wind gradients and effects of wind gradient slopes and non-linear profile variations on these patterns. Three-dimensional point-mass equations of motion are used, where the state variables include

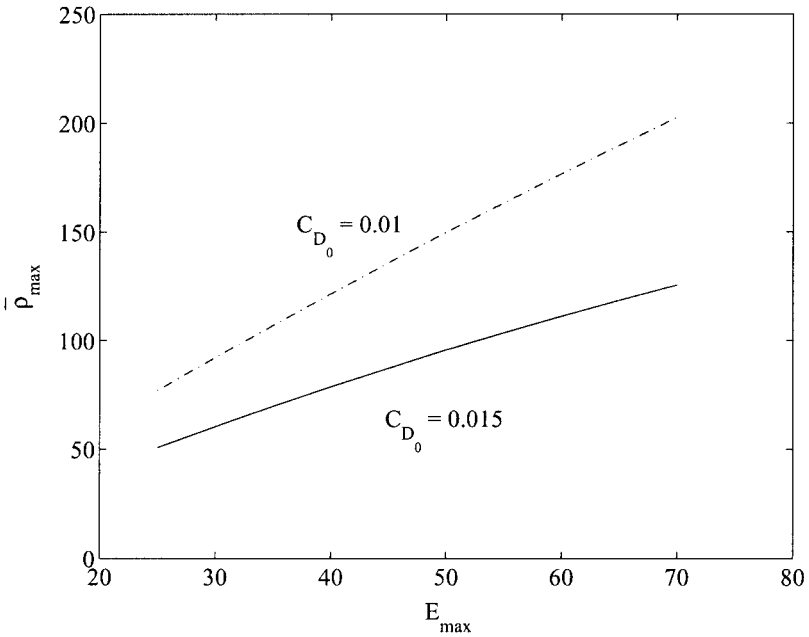

Figure 15. Least required wind gradient slopes for the basic soaring pattern.

airspeed, heading angle, flight path angle, east and north locations, and altitude, and the control variables include lift coefficient and glider bank angle. A single non-dimensional parameter describing the relative wind effect on dynamic soaring is identified that properly combines air density, wing loading, and wind gradient slope. Glider dynamic soaring flights are formulated as non-linear optimal control problems and three performance indices are used. The first one minimizes the cycle completion time whereas the second one maximizes the final altitude gain after a dynamic soaring cycle. In both problems, the initial airspeed, the initial heading angle, and the cycle time are open. The third one determines the least required wind gradient slope that can still sustain a powerless dynamic soaring flight. All formulations are subject to glider equations of motion, specified initial conditions, path constraints on states and controls, and appropriate terminal constraints that enforce periodic dynamic soaring flights of different patterns. Three fundamental patterns of dynamic soaring flights are considered: a basic pattern in which the final location is open, a travelling pattern in which the glider moves along the direction perpendicular to the wind, and a loiter pattern in which the glider circles around a fixed point. These optimal control problems are converted into parameter optimization via a collocation approach and solved numerically with the software NPSOL.

The three fundamental patterns of dynamic soaring require similar cycle times to complete, with the loiter pattern needing the longest time. When the final altitude is maximized, the basic dynamic soaring pattern can produce the largest final altitude gain, followed by the travelling dynamic soaring pattern. The loiter dynamic soaring produces the smallest possible final altitude gain of the three patterns. The average wind gradient slope significantly affects the peak altitude and final altitude gain in a dynamic soaring flight. Specifically, the smaller the wind

gradient slope is, the larger the peak altitude needs to be in order to complete a dynamic soaring flight. The least required wind gradient slope above which dynamic soaring is possible decreases as the aerodynamic efficiency increases or the parasitic drag coefficient decreases. For a given average wind gradient slope, a more logarithmic-like wind profile produces larger effective wind gradient slopes over low altitudes and is more favourable to dynamic soaring flights.

REFERENCES

1. Lange KO. Soaring meteorology. In *The Art of Gliding and Soaring*, Barringer LB (ed.). Pitman Publishing Corporation: London, 1942.
2. Arho R. Optimal dolphin soaring as a variational problem. *Technical Soaring* 1973; **3**(1):20–26.
3. Arho R. Some notes on soaring flight optimization theory. *Technical Soaring* 1976; **4**(2):27–30.
4. Metzger DE, Hedrick JK. Optimal flight paths for soaring flight. *Journal of Aircraft* 1975; **12**(11):867–871.
5. Pierson BL. Maximum altitude sailplane winch launch trajectories. *Aeronautical Quarterly* 1977; **28**;75–81.
6. Pierson BL, de Jong JL. Cross-country sailplane flight as a dynamic optimization problem. *International Journal for Numerical Methods in Engineering* 1978; **12**:1743–1759.
7. Pierson BL, Chen I. Minimum landing-approach distance for a sailplane. *Journal of Aircraft* 1979; **16**:287–288.
8. Pierson BL, Chen I. Minimum altitude-loss soaring in a specified vertical wind distribution. *Optimal Control Applications and Methods* 1980; **1**:205–215.
9. Litt FX, Sander G. Optimal flight strategy in a given space distribution of lifts with minimum and maximal altitude constraints. *Technical Soaring* 1981; **6**(2):23–28.
10. de Jong JL. The 'convex-combination approach', a geometric approach to the optimization of sailplane trajectories. *Technical Soaring* 1983; **8**(3):98–117.
11. de Jong JL. Instationary dolphin flight: the optimal energy exchange between a sailplane and vertical currents in the atmosphere. *Optimal Control Applications and Methods* 1985; **6**:113–124.
12. Lorenz J. Numerical solution of the minimum-time flight of a glider through a thermal by use of multiple shooting methods. *Optimal Control Applications and Methods* 1985; **6**:125–140.
13. Jenkins SA, Wasyl J. Optimization of glides for constant wind fields and course headings. *Journal of Aircraft* 1990; **27**(7):632–638.
14. Bridges PD. Alternative solution to optimum gliding velocity in a steady head wind to tail wind. *Journal of Aircraft* 1993; **30**(5):795–797.
15. Sachs G, Knoll A, Lesch K. Optimal utilization of wind energy for dynamic soaring 1991; **15**(2):49–55.
16. Kawabe H, Goto N. Modified direct optimization method for optimal control problems. *Theoretical and Applied Mechanics* 1999; **48**:225–234.
17. Stull RB. *An Introduction to Boundary Layer Meteorology*, Chapter 1. Kluwer Academic Publishers: Dordrecht, The Netherlands, 1988.
18. Kaimal JC, Finnigan JJ. *Atmospheric Boundary Layer Flows*, Chapter 1. Their Structure and Measurement. Oxford University Press: Oxford, 1994.
19. Speyer JL. Periodic optimal flight. *Journal of Guidance, Control, and Dynamics* 1996; **19**(4):745–754.
20. Hull D. Conversion of optimal control problems into parameter optimization problems. *Journal of Guidance, Control, and Dynamics* 1997; **20**(1):57–60.
21. Herman AL, Conway BA. Direct optimization using collocation based on high-order Gauss–Lobatto Quadrature rules. *Journal of Guidance, Control, and Dynamics* 1996; **19**(3):592–599.
22. Betts J. Survey of numerical methods for trajectory optimization. *Journal of Guidance, Control, and Dynamics* 1998; **21**(2):193–207.
23. Gill PE, Murray W, Saunders MA, Wright MH. User's guide for NPSOL (Version 4.0): a Fortran package for nonlinear programming. *Technical Report SOL* 86-2, Department of Operations Research, Stanford University, 1986.

